HHS Public Access

Author manuscript

Pflugers Arch. Author manuscript; available in PMC 2018 August 01.

Published in final edited form as:

Pflugers Arch. 2017 August ; 469(7-8): 965–974. doi:10.1007/s00424-017-2020-0.

Combined use of electron microscopy and intravital imaging captures morphological and functional features of podocyte detachment

James L. Burford[1], **Georgina Gyarmati**[1], **Isao Shirato**[2], **Wilhelm Kriz**[3], **Kevin V. Lemley**[4], and **János Peti-Peterdi**[1]

[1]Department of Physiology and Biophysics, Zilkha Neurogenetic Institute, University of Southern California, 1501 San Pablo Street, Room ZNI 335, Los Angeles, CA 90033, USA

[2]Division of Nephrology, Department of Internal Medicine, School of Medicine, Juntendo University, Tokyo, Japan

[3]Centre for Biomedicine and Medical Technology Mannheim (CBTM), Neuroanatomy, Medical Faculty Mannheim, Heidelberg University, Mannheim, Germany

[4]Division of Nephrology, Children's Hospital Los Angeles, CA, Los Angeles, USA

Abstract

The development of podocyte injury and albuminuria in various glomerular pathologies is still incompletely understood due to technical limitations in studying the glomerular filtration barrier (GFB) in real-time. We aimed to directly visualize the early morphological and functional changes of the GFB during the development of focal segmental glomerulosclerosis (FSGS) using a combination of transmission electron microscopy (TEM) and in vivo multiphoton microscopy (MPM) in the rat puromycin aminonucleoside (PAN) model. We hypothesized that this combined TEM + MPM experimental approach would provide a major technical improvement that would benefit our mechanistic understanding of podocyte detachment. Male Sprague-Dawley (for TEM) or Munich-Wistar-Frömter (for MPM) rats were given a single dose of 100–150 mg/kg body weight PAN i.p. and were either sacrificed and the kidneys processed for TEM or surgically instrumented for in vivo MPM imaging at various times 2–14 days after PAN administration. Both techniques demonstrated hypertrophy and cystic dilatations of the subpodocyte space that developed as early as 2–3 days after PAN. Adhesions of the visceral epithelium to the parietal Bowman's capsule (synechiae) appeared at days 8–10. TEM provided unmatched resolution of podocyte foot process remodeling, while MPM revealed the rapid dynamics of pseudocyst filling, emptying, and rupture, as well as endothelial and podocyte injury, misdirected filtration, and

Correspondence to: János Peti-Peterdi.

Electronic supplementary material The online version of this article (doi:10.1007/s00424-017-2020-0) contains supplementary material, which is available to authorized users.

Authors' contributions JPP and WK designed the experiments. JLB, GG, and IS performed the experiments and analyzed the data. JPP, KL, and WK interpreted the results and wrote the manuscript.

Compliance with ethical standards The experimental protocols for the in vivo experiments were approved by the Institutional Animal Care and Use Committee of the University of Southern California; the structural studies were conducted in accordance with the National Research Council guidlines for the Care and Use of laboratory animals of Juntendo University, Tokyo.

Conflict of interest The authors declare that they have no conflict of interest.

podocyte shedding. Due to the complementary advantages of TEM and MPM, this combined approach can provide an unusually comprehensive and dynamic portrayal of the alterations in podocyte morphology and function during FSGS development. The results advance our understanding of the role and importance of the various cell types, hemodynamics, and mechanical forces in the development of glomerular pathology.

Keywords

Podocyte; Glomerulus; Puromycin; Glomerulosclerosis; Intravital microscopy

Introduction

The mechanistic understanding of important glomerular disease processes including the development of albuminuria and glomerulosclerosis has been limited due to the technical difficulty in studying the glomerular filtration barrier (GFB) in real-time. Podocytes are one of the key cell types of the GFB and play important roles in the maintenance of the normal healthy GFB and in the development of glomerular pathologies. However, podocytes are rather inaccessible renal cell types that have been traditionally studied in cultured cell systems in vitro and in fixed static tissue samples [12, 23]. For the highest resolution imaging of podocyte architecture, scanning and transmission electron microscopies (TEM) have been the gold standard methods for decades [7, 8, 10, 12, 20]. In fact, our current knowledge and mechanistic understanding of the processes of podocyte injury and detachment are largely based on TEM [12, 14, 18].

However, TEM of fixed renal tissues has obvious inherent limitations for studying dynamic processes of the living kidney and podocytes. For the study of podocytes in vivo in the intact kidney, different modalities of intravital multiphoton microscopy (MPM) have emerged in the past few years [2, 5, 6, 9, 24–26, 32]. Thanks to MPM, it is now possible not only to study the three-dimensional architecture and cellular complexity of the GFB [5, 27] but also most importantly to quantitatively visualize the many dynamic functional features of glomerular filtration [2, 9], capillary blood flow [2, 9, 24, 27], albumin leakage [1, 21, 27, 30, 32], podocyte calcium [1], motility [1, 5, 27, 34], and detachment in vivo [27]. Also, the interactions between glomerular endothelial and mesangial cells and podocytes in the intact living rat and mouse kidney can be visualized with MPM in great detail [27].

With the ultimate goal of improving our understanding of the mechanisms of glomerular pathology and albuminuria development, several animal models of glomerular injury including focal segmental glomerulosclerosis (FSGS) have been developed. In the present work, the puromycin aminonucleoside (PAN) model of FSGS, a classic rat model of glomerular pathology [7, 8, 10], was used with a special imaging approach that combined TEM and in vivo MPM studies. The purpose of this study was to provide a comprehensive and dynamic portrayal of the alterations in podocyte ultrastructure (with both TEM and MPM) and correlate these with the temporal features of podocyte detachment and GFB dysfunction (with MPM) in the intact living kidney during FSGS development. We

hypothesized that this combined TEM + MPM experimental approach would improve our mechanistic understanding of podocyte detachment and glomerular pathologies.

Methods

Experimental protocol and animals

The experimental protocols for the in vivo experiments were approved by the Institutional Animal Care and Use Committee of the University of Southern California; the structural studies were conducted in accordance with the National Research Council guidlines for the Care and Use of laboratory animals of Juntendo University, Tokyo. As described before male Sprague-Dawley (for TEM) or Munich-Wistar-Fromter (for MPM) rats (200–450 g, Harlan, Madison, WI) were given a single dose of 100 mg/kg body weight PAN i.p. (in vivo studies), or 150 mg/kg body weight (in structural studies) [10], and were either sacrificed and the kidneys processed for transmission electron microscopy (TEM) or surgically instrumented for in vivo MPM imaging at various times 2–14 days after PAN.

Transmission electron microscopy

Male Sprague-Dawley rats treated with PAN were sacrificed, and the kidneys processed for TEM as described previously [7, 8, 20]. Briefly, under pentobarbital anesthesia and without preceding flushing of the vasculature, the animals were directly perfused with a 1.0% glutaraldehyde, 0.1 M phosphate buffer (pH 7.3) solution for 4 min through a retrograde cannula inserted into the abdominal aorta. Cortical tissue of the kidneys was excised with razor blades as 2 × 2 × 3 mm pieces and immersed in the same fixative at 4 °C for 2 h, subsequently postfixed in 1% osmium tetroxide for 1 h. After washing with 0.1 M phosphate buffer (pH 7.3), the tissue was processed for TEM by standard procedures and embedded in Epon 812. Ultrathin sections were cut on an Ultracut E microtome (Reichert-Jung, Nussloch, Germany), stained with uranyl acetate and lead citrate and examined with a Philips 301 electron microscope at 80 kV.

Multiphoton microscopy

Munich-Wistar-Fromter rats were anesthetized with thiobutabarbital (Inactin, 130 mg/kg body wt, Sigma). A trachea tube was placed to facilitate breathing, and the right carotid artery was cannulated for dye infusions. Alexa Fluor 594-conjugated bovine serum albumin (100 μl of a 10 mg/ml stock in iv bolus, Invitrogen) was injected i.v. to label the vasculature. Lucifer yellow (LY), a 0.4-kD freely filterable, but cell membrane impermeable, small molecule was infused continuously into the carotid artery (10 μl/min of 12.5 mg/ml stock solution, Invitrogen) to label the primary filtrate in the Bowman’s space. In some experiments, the cell nuclei were labeled using Hoechst33342 (100 μl of a 25 mg/ml stock in iv bolus, Invitrogen). The left kidney was exteriorized through a flank incision, and the animal was placed on the microscope stage as described previously [9]. Body temperature was maintained with a homeothermic blanket system (Harvard Apparatus). Optical sectioning of the intact kidney in vivo was performed using a Leica TCS SP5 multiphoton confocal fluorescence imaging system (Leica Microsystems, Heidelberg, Germany) with a × 63 Leica glycerine-immersion objective (NA 1.3) powered by a Chameleon Ultra-II MP laser at 860–920 nm (coherent) and a DMI 6000 inverted microscope’s external

nondescanned detectors with TRITC (red channel) and FITC (green channel) filters. Fluorescence intensity measurements were performed in time-lapse (xyt) mode in multiple regions of interest (ROI) in the Bowman's space, the podocyte pseudocysts, and the periglomerular interstitium. Pseudocyst volume changes were measured based on detecting LY or Alexa594-Albumin fluorescence pixel numbers in ROIs drawn closely over the largest pseudocyst perimeter using the Quantify package of LAS AF Lite software (2.0.2 build 2038, Leica Microsystems).

Results

To visualize the development and the different stages of podocyte injury in the commonly used PAN rat model, the animals were either sacrificed and the kidneys processed for TEM or surgically instrumented for in vivo MPM imaging at various times 2–14 days after PAN. TEM performed on tissue samples harvested 4 and 8 days after PAN treatment showed stereotypical changes in podocyte and glomerular architecture that involved all glomeruli and always the entire glomerulus as illustrated in Fig. 1a. Most prominent were the appearance of numerous podocyte pseudocysts and the wide replacement of the pattern of interdigitating foot processes by "foot process effacement (FPE)"already 4 days after PAN treatment. Thus, the floor of most pseudocysts was covered by FPE; in some areas and also in some pseudocysts, a normal interdigitating FP-pattern was still seen (Fig. 1b, c). The content of pseudocysts varied in density likely reflecting different albumin concentrations of cyst fluid. At various sites, but not ubiquitously, podocytes contained accumulations of vacuoles filled with a homogenous matrix of various density (Fig. 1c).

After 8 days of treatment, a dramatic progression of damages was seen (Fig. 1d–f). A normal FP pattern was no longer visible. Instead and in addition to an ubiquitous occurrence of FPE, circumscribed glomerular basement membrane (GBM) areas deprived of any podocyte cover were encountered at many sites (Fig. 1d). This disconnection of podocyte processes from the GBM must be considered as the starting injury of podocyte detachment. Overarching those bare GBM areas, a second type of small pseudocysts developed, the floor of which consisted of naked GBM. Since all the cyst spaces were in communication with each other at many sites, filtrate from behind the GBM into Bowman's space had to pass these labyrinthine spaces. Prominent at this stage of damage were also the varying forms of adhesions of the tuft to Bowman's capsule (Fig. 1e, f). The nidus for the formation of a tuft adhesion to Bowman's capsule consists of the touch of a podocyte, most frequently of one of its pseudocysts with the parietal epithelium. This contact will progress to adhesions/crescents of great variability in their composition of capillary loops, podocytes, parietal epithelial cells, parietal basement membrane (PBM), and other extracellular matrices as well as interstitial cells. Two of those adhesions are shown in Fig. 1e, f, whereas in Fig. 1e, a barrier of cells and PBM between Bowman's space and the interstitium is still present. In Fig. 1f there seems to be a free communication between both compartments.

Intravital MPM imaging performed at varying times after PAN treatment perfectly replicated the above findings on podocyte structural alterations. The use of fluorescent tracer molecules allowed us to label and clearly identify the different anatomical (e.g., cell nuclei) and fluid compartments within the glomerulus (e.g., the capillary plasma and Bowman's space) and to

track the permeability of high MW (albumin) and low MW (Lucifer yellow, LY) plasma markers through the GFB. We found that the vascular endothelium and mesangial cells endocytosed LY intensely and therefore these cells were labeled, as opposed to normal podocytes and parietal cells that did not show any signs of dye uptake and remained dark and unlabeled during the MPM imaging sessions (Fig. 2a). Earlier MPM imaging work from our laboratory described the aging-related, spontaneously developing glomerular pathology that is typical of old Munich-Wistar-Fromter rats [30]. In the present work, the use of gender and age-matched rats that have not been treated with PAN confirmed the lack of obvious, pre-existing glomerular pathology (Fig. 2a).

In contrast to normal glomerular structure (Fig. 2a), a few podocytes showed enlarged, balled up shape of cell body (large dark cells around the glomerular capillaries) as the first sign of injury within 2–3 days after PAN (Fig. 2b). Numerous small and large pseudocysts, which contained LY-labeled fluid, developed in podocytes by 4 days after PAN treatment (Fig. 2c). Over time, as a reflection and functional readout of the level of GFB integrity under the pseudocysts, the fluorescence of cyst fluid became variable. Green (LY containing), yellow (mixed), and red (albumin containing) pseudocysts were all present around the entire glomerulus (Fig. 2d–f). The largest podocyte pseudocysts, as the core structure, formed focal adhesions of the glomerular tuft to the parietal Bowman's capsule (synechiae) 7–10 days after PAN (Fig. 2d, e). Intact, healthy podocytes (normal shape and no albumin permeability) were also observed making contact with parietal cells in other glomerular regions, but never developed synechiae. Numerous densely packed small cells that appeared to be migrating were observed on the outside of the core cysts, forming a continuous cell layer (bridge) between podocytes and parietal cells (Fig. 2e). Injured podocytes around the synechiae contained green/yellow/red-labeled intracellular vesicles (Fig. 1e), while this was never observed in healthy looking podocytes in other glomerular regions. The GBM was also identified and visible with MPM based on its green labeling by LY (Fig. 2e). In later stages (14 days after PAN), crescent-like multilayered Bowman's capsules consisting of numerous cells and LY-filled fluid spaces were found surrounding barely perfused glomeruli (Fig. 2f).

To quantitatively visualize the dynamic temporal changes of stereotypical pathological features including pseudocyst volume, misdirected filtration, and podocyte shedding, time-lapse MPM imaging of the same glomeruli was performed for several minutes. When the same optical section of glomeruli at constant depth was observed over time, MPM imaging identified several albumin-containing pseudocysts with steady-state volume. However, numerous pseudocysts showed either single or regularly oscillating episodes of filling and emptying as illustrated in Supplement movie 1 and in Fig. 3a–c. Analysis of the temporal profile of podocyte pseudocyst volume changes (Fig. 3c) confirmed the variability of this phenomenon, with random filling or emptying of some but not all pseudocysts, and multiple volume oscillations (one in every 10–60 s) in a few pseudocysts.

Time-lapse in vivo MPM imaging also visualized the presence and rapid dynamics of misdirected filtration after PAN treatment. Bolus injection of the freely filtered LY into the carotid artery labeled the passage of primary filtrate not only into the proximal tubule but also into specific focal interstitial regions outside the glomerulus, usually adjacent to an

existing synechia (Fig. 4a–c; Supplement movie 2). Analysis of the temporal profile of LY fluorescence intensity changes (Fig. 4e) showed that the glomerular filtrate passes into Bowman's capsule/proximal tubule and the periglomerular focal interstitium essentially simultaneously. In addition, not only the low MW LY but also the high MW albumin is filtered into the periglomerular interstitium, which is taken up by numerous cells surrounding the region around the synechia (Fig. 4d). Glomerular leakage and proximal tubule uptake of albumin were also visible after PAN treatment (Fig. 4d). Optical sectioning (z-stack) of the synechia shown in Fig. 4d is available in Supplement movie 3.

Finally, MPM was used to visualize the development of structural changes and dynamics of podocyte shedding. Time-lapse images captured the rapid and significant enlargement and rupture of pseudocysts within 60 s, as well as the shedding of cell debris (Fig. 5a–c; Supplement movies 4–5). On multiple occasions, endothelial cell detachment and microthrombi were observed in the glomerular capillary directly adjacent to the injured podocyte, which appeared to form prior to pseudocyst expansion and podocyte shedding (Fig. 5a–c; Supplement movies 4–5). Albumin-containing vesicles were also found shedding into the filtrate in the Bowman's space (Fig. 5d). Analysis of the dynamic changes in podocyte pseudocyst volume (Fig. 5e) found rapid and robust, approximately tenfold expansion in volume within 60 s.

Discussion

The present study performed a comprehensive morphological and functional analysis of the development of PAN-induced glomerular pathology in the rat kidney, with the goal to improve our mechanistic understanding of the underlying disease processes. For the first time, TEM of fixed histological renal tissue sections was combined with separate intravital MPM imaging performed over the same time period in the same rat PAN model of FSGS. This experimental approach represents a major technical improvement for the kidney and podocyte research, because it combines the unique advantages of the two imaging techniques, high spatial resolution of glomerular ultrastructure (with TEM), and time-lapse functional analysis of the intact living kidney (with intravital MPM). Accordingly, this study provided new visual clues and mechanistic insights on podocyte injury and detachment, allowed us to make GFB structure-function correlations, and established new temporal features of the development of podocyte and glomerular dysfunction. None of the currently available other experimental approaches and techniques are capable of achieving these.

There is full agreement in the depiction of the alterations in glomerular and podocyte architecture after PAN treatment between TEM and in vivo MPM. The changes as seen by TEM largely correspond to the changes in other glomerular disease models in rats progressing to FSGS [12, 14], including unilateral nephrectomy [20], DOCA-salt-hypertension [11], growth stimulation by FGF2 treatment [13], Masugi nephritis [12, 14, 18, 20, 33], etc. The stereotypical course of damage progression in these quite different models is accounted for (i) that a failure of the podocyte is the common culprit and (ii) that, though the risks of podocyte failure are different, finally mechanical forces (tensile and shear stress of filtration) lead to the process of the gradual detachment of injured podocytes. The first step in this process is FPE, a protective response of podocytes to decrease their susceptibility

to a disconnection from the GBM [12, 14, 18, 20]. If this measure fails, local detachments of FPs will lead to uncontrolled filtrate flows through bare areas of GBM (Fig. 1d). Thereafter, the filtrate has to pass the intricate subpodocyte spaces (i.e., the communicating system of pseudocysts) before reaching Bowman's space. On this way, the dynamic forces of flow will tend to drag podocytes toward the urinary orifice. Pseudocysts develop in all of the abovementioned models; they seem to be very prominent in the PAN model.

Adhesions of the tuft to Bowman's capsule followed by crescent formation represents the unifying mechanism how a glomerular disease encroaches upon the tubulo-interstitium and progresses to the loss of the entire nephron. The formation of tuft adhesions/synechiae appears to be a slow process. Time-lapse MPM imaging of several early-phase adhesions for several hours showed no obvious morphological or functional changes associated with their development (not shown). The formation of a tuft adhesion starts with the establishment of bridges between the tuft and Bowman's capsule involving podocytes and parietal cells as first shown in an inflammatory model [19]. Recent genetic cell fate mapping studies have confirmed these results and clarified the role of podocytes and parietal epithelial cells as well as the interaction between both in more detail [5, 36]. When comparing various models or even individual manifestations in the same model, the courses from the initial touch between podocyte and parietal cells to the encroachment onto the tubulo-interstitium seem to be very variable. With respect to the present results in the PAN model, the early break of the parietal barrier including the PBM (Fig. 1f) was surprising but fully agreed with the MPM observations (Figs. 4 and 5).

The combination of TEM and MPM in the present study proved to be highly valuable for improving our understanding of glomerular pathology development. Due to their unique and complementary advantages, TEM provided unmatched resolution of podocyte foot process remodeling after PAN (Fig. 1; a capability that MPM does not have), while MPM revealed the rapid dynamics of pseudocyst filling, emptying, and rupture, endothelial and podocyte injury, misdirected filtration, and podocyte shedding (Figs. 2, 3, 4, and 5; capabilities that TEM does not have). One example for the benefit of such a combined approach is the better understanding of pseudocyst development, function, and albumin permeability. TEM found variability of GFB ultrastructure at the base of pseudocysts after PAN (normal, effaced, and bare GBM areas) and varying density of cyst content that likely reflected different albumin concentrations of cyst fluid (Fig. 1c, d). Intravital MPM confirmed this functionally by the visualization of green (LY containing), yellow (mixed), and red (albumin containing) pseudocysts that were all found within a single glomerulus (Fig. 2d–f) and likely reflected the level of GFB integrity under the pseudocysts (normal/partly effaced, partly effaced/bare GBM, mainly bare GBM, respectively). Also, the observation of different density vesicles with TEM (Fig. 1c, d) and green/yellow/red-labeled intracellular vesicles in injured podocytes around synechiae with MPM (Fig. 2e) suggested that in addition to lysosomes, injured podocytes have LY and albumin-containing endosomes. For additional benefit and synergy between the two techniques, future work may expand the combined TEM + MPM approach to studies in the same animal, i.e., MPM intravital imaging followed by TEM analysis upon fixation of the same kidney.

Time-lapse in vivo MPM imaging visualized the dynamics of pseudocyst filling, emptying, and rupture, as well as endothelial and podocyte injury, misdirected filtration, and podocyte shedding. Supplement movies 1, 2, 3, 4, and 5 demonstrate these processes and their respective figures (Figs. 2, 3, 4, and 5) provide quantitative analysis of their dynamic features. The reversible filling and emptying of large pseudocysts, especially those that showed slow regular oscillations in cyst volume every 10–60 s (Fig. 3c) suggest that this phenomenon is linked to the constantly oscillating high glomerular hemodynamic forces that podocytes are physiologically exposed to. Using MPM imaging, we recently visualized the two-component oscillations in single nephron GFR and glomerular blood flow with faster (cycle time about 10 s) and slower (cycle time about 50 s) elements that are consequences of the afferent arteriole myogenic and tubuloglomerular feedback (TGF) mechanisms, respectively [9, 27]. The closing of the narrow exit clefts from the “subcellbody spaces” (later called subpodocyte spaces (SPS) [22]) that lead to a bulging of podocyte cell bodies has first been shown in an UNX model of FSGS [20]. The opening/closing of these clefts may also be involved in pseudocyst volume changes. Previous MPM imaging studies confirmed that podocyte pseudocysts are large dilatations of the recently re-discovered SPS [27], a labyrinthine fluid space between the underside of the podocyte cell body and the foot processes [22, 31].

The other, potentially even more robust hemodynamic (mechanical) force behind pseudocyst volume expansion could be the acute elevations in glomerular capillary pressure due to the formation of local capillary microthrombi. MPM imaging observed that the most robust expansions and eventually the rupture of pseudocysts were almost always associated with prior formation of small, focal microthrombi in the adjacent glomerular capillary (Fig. 5; Supplement movies 4–5). The focal thrombotic microangiopathy may be the result of direct endothelial toxicity of PAN (similarly to the effect of adriamycin in mouse models [37]) or secondarily due to podocyte injury. The interdependence of podocyte-endothelium dysfunction and injury that involves microthrombus formation has been visualized with MPM in an earlier report [27]. Also, recent works reported the importance of glomerular endothelial mitochondrial dysfunction and disruption of the endothelial glycocalyx in endothelial and podocyte crosstalk, albuminuria, and glomerulosclerosis development [4, 28]. Based on the data shown in Fig. 5 and in Supplement movies 4–5, the sudden rupture of a large pseudocyst seems to have the effect of a dam break, leading to enormous filtrate flows and filling of the small pseudocysts that then start the final process of podocyte detachment. The high local filtrate flows that occur when the pseudocyst opens, will be associated with dramatic increases in shear stress and, possibly, this challenge is crucial for podocyte detachment. In fact, the critical pathogenic importance of podocyte shear stress created by the filtrate flow was recently reported and discussed [15–17]. The above listed GFB and capillary forces, the constantly oscillating local hemodynamics, interdependence with endothelial injury and microthrombi, the continuous filling and emptying (and rupture) of podocyte pseudocysts, and the shear stress of filtration all emphasize the key role of mechanical factors in podocyte detachment.

The use of several fluorescent plasma and fluid tracers for MPM imaging studies has been described previously [2, 9, 21, 24, 27, 35]. LY is a valuable and easy to use fluid marker that is freely filtered, and has been used in the past to visualize the glomerular filtration process,

Bowman's space, glomerular epithelial cells (in negative) and to quantitate SNGFR [9, 27, 29]. LY was used in conjunction with the rat PAN model in a recent preliminary work [27]. In the present study, LY was used to help visualize glomerular architecture (Fig. 2) and the process of misdirected filtration (Fig. 4), a classic phenomenon in the injured glomerulus where tuft adhesions (synechiae) are present [12]. Figure 4a–c, e demonstrates that the filtration into the periglomerular interstitial area around a synechia is essentially simultaneous with filtration into the Bowman's space and to the early proximal tubule. This suggests minimal resistance of the synechia wall to fluid flow corroborating with TEM observations (Fig. 1f). Importantly, focal leakage of albumin to the interstitium surrounding the tuft adhesion was also present. Consistent with the pathogenic effect of interstitial albumin, several periglomerular cells in the synechia area (likely immune cells) appeared to endocytose albumin (Fig. 4d). Recent MPM imaging and other experiments showed albumin endocytosis by podocytes [3, 32] as well as the release of these albumin-vesicles into the urinary space [32]. The present study confirmed the presence and passage of albumin-containing vesicles in the Bowman's space in the rat PAN model. A recent report documented the rupture of albumin-containing pseudocysts that resulted in the emptying of the high albumin-containing cyst fluid into the Bowman's space and downstream the nephron [25]. Albumin endocytosis by injured podocytes and the rupture of albumin-containing large pseudocysts are likely alternative mechanisms of albumin leakage through the GFB that contribute to the development of albuminuria.

In summary, the present study used a combined TEM + MPM experimental approach and captured classic morphological and new functional and temporal features of the development of podocyte injury. This combined approach provides major technical improvements over earlier methods and improves the mechanistic understanding of glomerular pathologies. Since intravital MPM has become a widely available and commonly used experimental technique included in kidney research, future applications of similar combined TEM + MPM approaches are feasible and practical for studying other models of glomerular and kidney diseases.

Acknowledgments

This work was supported in part by the US National Institutes of Health grants DK064324 and DK100944 to J.P-P.

References

1. Burford JL, Villanueva K, Lam L, Riquier-Brison A, Hackl MJ, Pippin J, Shankland SJ, Peti-Peterdi J. Intravital imaging of podocyte calcium in glomerular injury and disease. J Clin Invest. 2014; 124:2050–2058. DOI: 10.1172/jci71702 [PubMed: 24713653]
2. Dunn KW, Sandoval RM, Kelly KJ, Dagher PC, Tanner GA, Atkinson SJ, Bacallao RL, Molitoris BA. Functional studies of the kidney of living animals using multicolor two-photon microscopy. Am J Physiol—Cell Physiol. 2002; 283:C905–C916. DOI: 10.1152/ajpcell.00159.2002 [PubMed: 12176747]
3. Eyre J, Ioannou K, Grubb BD, Saleem MA, Mathieson PW, Brunskill NJ, Christensen EI, Topham PS. Statin-sensitive endocytosis of albumin by glomerular podocytes. Am J Physiol Renal Physiol. 2007; 292:F674–F681. DOI: 10.1152/ajprenal.00272.2006 [PubMed: 17032937]
4. Garsen M, Lenoir O, Rops AL, Dijkman HB, Willemsen B, van Kuppevelt TH, Rabelink TJ, Berden JH, Tharaux PL, van der Vlag J. Endothelin-1 induces proteinuria by heparanase-mediated

disruption of the glomerular glycocalyx. J Am Soc Nephrol. 2016; 27:3545–3551. DOI: 10.1681/asn.2015091070 [PubMed: 27026367]

5. Hackl MJ, Burford JL, Villanueva K, Lam L, Susztak K, Schermer B, Benzing T, Peti-Peterdi J. Tracking the fate of glomerular epithelial cells in vivo using serial multiphoton imaging in new mouse models with fluorescent lineage tags. Nat Med. 2013; 19:1661–1666. DOI: 10.1038/nm.3405 [PubMed: 24270544]
6. Hall AM, Schuh CD, Haenni D. New frontiers in intravital microscopy of the kidney. Curr Opin Nephrol Hypertens. 2017; 26:172–178. DOI: 10.1097/mnh.0000000000000313 [PubMed: 28198734]
7. Inokuchi S, Sakai T, Shirato I, Tomino Y, Koide H. Ultrastructural changes in glomerular epithelial cells in acute puromycin aminonucleoside nephrosis: a study by high-resolution scanning electron microscopy. Virchows Arch A Pathol Anat Histopathol. 1993; 423:111–119. [PubMed: 8212539]
8. Inokuchi S, Shirato I, Kobayashi N, Koide H, Tomino Y, Sakai T. Re-evaluation of foot process effacement in acute puromycin aminonucleoside nephrosis. Kidney Int. 1996; 50:1278–1287. [PubMed: 8887289]
9. Kang JJ, Toma I, Sipos A, McCulloch F, Peti-Peterdi J. Quantitative imaging of basic functions in renal (patho)physiology. Am J Physiol Renal Physiol. 2006; 291:F495–F502. DOI: 10.1152/ajprenal.00521.2005 [PubMed: 16609147]
10. Kim YH, Goyal M, Kurnit D, Wharram B, Wiggins J, Holzman L, Kershaw D, Wiggins R. Podocyte depletion and glomerulosclerosis have a direct relationship in the PAN-treated rat. Kidney Int. 2001; 60:957–968. DOI: 10.1046/j.1523-1755.2001.060003957.x [PubMed: 11532090]
11. Kretzler M, Koeppen-Hagemann I, Kriz W. Podocyte damage is a critical step in the development of glomerulosclerosis in the uninephrectomised-desoxycorticosterone hypertensive rat. Virchows Arch. 1994; 425:181–193. [PubMed: 7952502]
12. Kriz W, Gretz N, Lemley KV. Progression of glomerular diseases: is the podocyte the culprit? Kidney Int. 1998; 54:687–697. DOI: 10.1046/j.1523-1755.1998.00044.x [PubMed: 9734594]
13. Kriz W, Hahnel B, Hosser H, Rosener S, Waldherr R. Structural analysis of how podocytes detach from the glomerular basement membrane under hypertrophic stress. Front Endocrinol (Lausanne). 2014; 5:207.doi: 10.3389/fendo.2014.00207 [PubMed: 25566184]
14. Kriz W, LeHir M. Pathways to nephron loss starting from glomerular diseases-insights from animal models. Kidney Int. 2005; 67:404–419. DOI: 10.1111/j.1523-1755.2005.67097.x [PubMed: 15673288]
15. Kriz W, Lemley KV. A potential role for mechanical forces in the detachment of podocytes and the progression of CKD. J Am Soc Nephrol. 2015; 26:258–269. DOI: 10.1681/asn.2014030278 [PubMed: 25060060]
16. Kriz W, Lemley KV. Mechanical challenges to the glomerular filtration barrier: adaptations and pathway to sclerosis. Pediatr Nephrol. 2017; 32:405–417. DOI: 10.1007/s00467-016-3358-9 [PubMed: 27008645]
17. Kriz W, Lemley KV. Potential relevance of shear stress for slit diaphragm and podocyte function. Kidney Int. 2017; 91:1283–1286. DOI: 10.1016/j.kint.2017.02.032 [PubMed: 28501303]
18. Kriz W, Shirato I, Nagata M, LeHir M, Lemley KV. The podocyte's response to stress: the enigma of foot process effacement. Am J Physiol Renal Physiol. 2013; 304:F333–F347. DOI: 10.1152/ajprenal.00478.2012 [PubMed: 23235479]
19. Le Hir M, Keller C, Eschmann V, Hahnel B, Hosser H, Kriz W. Podocyte bridges between the tuft and Bowman's capsule: an early event in experimental crescentic glomerulonephritis. J Am Soc Nephrol. 2001; 12:2060–2071. [PubMed: 11562404]
20. Nagata M, Kriz W. Glomerular damage after uninephrectomy in young rats. II. Mechanical stress on podocytes as a pathway to sclerosis. Kidney Int. 1992; 42:148–160. [PubMed: 1635344]
21. Nakano D, Kobori H, Burford JL, Gevorgyan H, Seidel S, Hitomi H, Nishiyama A, Peti-Peterdi J. Multiphoton imaging of the glomerular permeability of angiotensinogen. J Am Soc Nephrol. 2012; 23:1847–1856. DOI: 10.1681/asn.2012010078 [PubMed: 22997258]

22. Neal CR, Crook H, Bell E, Harper SJ, Bates DO. Three-dimensional reconstruction of glomeruli by electron microscopy reveals a distinct restrictive urinary subpodocyte space. J Am Soc Nephrol. 2005; 16:1223–1235. DOI: 10.1681/asn.2004100822 [PubMed: 15829713]
23. Pavenstadt H, Kriz W, Kretzler M. Cell biology of the glomerular podocyte. Physiol Rev. 2003; 83:253–307. DOI: 10.1152/physrev.00020.2002 [PubMed: 12506131]
24. Peti-Peterdi J, Burford JL, Hackl MJ. The first decade of using multiphoton microscopy for high-power kidney imaging. Am J Physiol Renal Physiol. 2012; 302:F227–F233. DOI: 10.1152/ajprenal.00561.2011 [PubMed: 22031850]
25. Peti-Peterdi J, Kidokoro K, Riquier-Brison A. Novel in vivo techniques to visualize kidney anatomy and function. Kidney Int. 2015; 88:44–51. DOI: 10.1038/ki.2015.65 [PubMed: 25738253]
26. Peti-Peterdi J, Kidokoro K, Riquier-Brison A. Intravital imaging in the kidney. Curr Opin Nephrol Hypertens. 2016; 25:168–173. DOI: 10.1097/mnh.0000000000000219 [PubMed: 27008595]
27. Peti-Peterdi J, Sipos A. A high-powered view of the filtration barrier. J Am Soc Nephrol. 2010; 21:1835–1841. DOI: 10.1681/asn.2010040378 [PubMed: 20576805]
28. Qi H, Casalena G, Shi S, Yu L, Ebefors K, Sun Y, Zhang W, D'Agati V, Schlondorff D, Haraldsson B, Bottinger E, Daehn I. Glomerular endothelial mitochondrial dysfunction is essential and characteristic of diabetic kidney disease susceptibility. Diabetes. 2017; 66:763–778. DOI: 10.2337/db16-0695 [PubMed: 27899487]
29. Rosivall L, Mirzahosseini S, Toma I, Sipos A, Peti-Peterdi J. Fluid flow in the juxtaglomerular interstitium visualized in vivo. Am J Physiol Renal Physiol. 2006; 291:F1241–F1247. DOI: 10.1152/ajprenal.00203.2006 [PubMed: 16868308]
30. Salmon AH, Ferguson JK, Burford JL, Gevorgyan H, Nakano D, Harper SJ, Bates DO, Peti-Peterdi J. Loss of the endothelial glycocalyx links albuminuria and vascular dysfunction. J Am Soc Nephrol: JASN. 2012; 23:1339–1350. DOI: 10.1681/asn.2012010017 [PubMed: 22797190]
31. Salmon AH, Toma I, Sipos A, Muston PR, Harper SJ, Bates DO, Neal CR, Peti-Peterdi J. Evidence for restriction of fluid and solute movement across the glomerular capillary wall by the subpodocyte space. Am J Physiol Renal Physiol. 2007; 293:F1777–F1786. DOI: 10.1152/ajprenal.00187.2007 [PubMed: 17804486]
32. Schiessl IM, Hammer A, Kattler V, Gess B, Theilig F, Witzgall R, Castrop H. Intravital imaging reveals angiotensin II-induced transcytosis of albumin by podocytes. J Am Soc Nephrol. 2016; 27:731–744. DOI: 10.1681/asn.2014111125 [PubMed: 26116357]
33. Shirato I, Hosser H, Kimura K, Sakai T, Tomino Y, Kriz W. The development of focal segmental glomerulosclerosis in masugi nephritis is based on progressive podocyte damage. Virchows Arch. 1996; 429:255–273. [PubMed: 8972762]
34. Siegerist F, Zhou W, Endlich K, Endlich N. 4D in vivo imaging of glomerular barrier function in a zebrafish podocyte injury model. Acta Physiol (Oxf). 2017; 220:167–173. DOI: 10.1111/apha.12754 [PubMed: 27414464]
35. Sipos A, Toma I, Kang JJ, Rosivall L, Peti-Peterdi J. Advances in renal (patho)physiology using multiphoton microscopy. Kidney Int. 2007; 72:1188–1191. DOI: 10.1038/sj.ki.5002461 [PubMed: 17667980]
36. Smeets B, Uhlig S, Fuss A, Mooren F, Wetzels JF, Floege J, Moeller MJ. Tracing the origin of glomerular extracapillary lesions from parietal epithelial cells. J Am Soc Nephrol: JASN. 2009; 20:2604–2615. DOI: 10.1681/ASN.2009010122 [PubMed: 19917779]
37. Sun YB, Qu X, Zhang X, Caruana G, Bertram JF, Li J. Glomerular endothelial cell injury and damage precedes that of podocytes in adriamycin-induced nephropathy. PLoS One. 2013; 8:e55027.doi: 10.1371/journal.pone.0055027 [PubMed: 23359116]

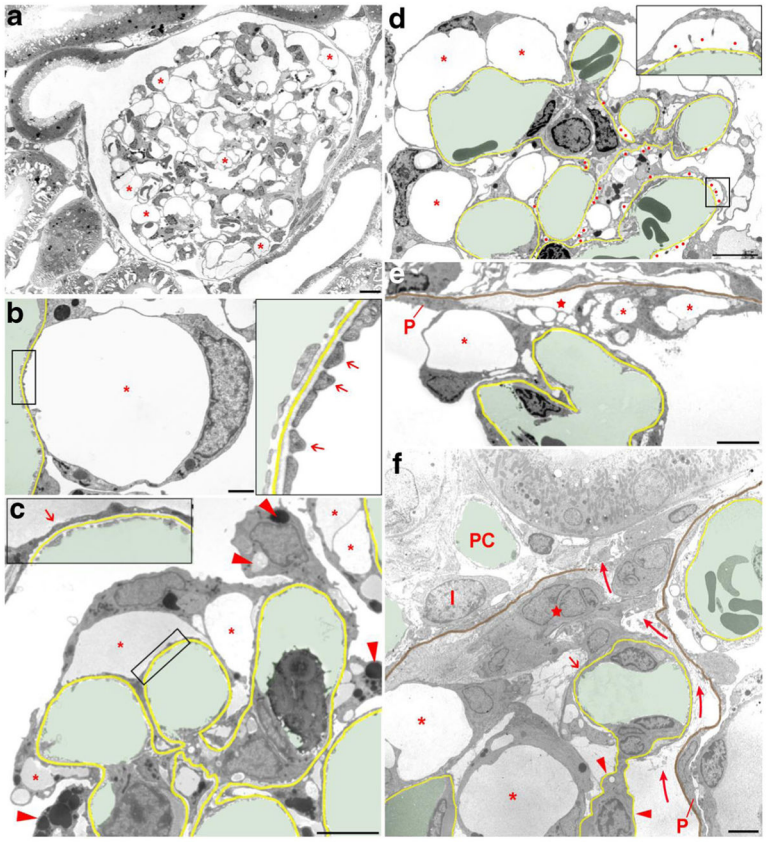

Fig. 1.

Transmission electron micrographs illustrating changes in podocyte morphology after puromycin aminonucleoside (PAN) treatment. In **b–f**, the GBM is highlighted in *yellow*, capillary lumens in *green*; in **e** and **f**, in addition, the parietal basement membrane (PBM) is shown in *brown*. **a** Overview of a whole glomerular profile showing that podocyte pseudocyst (*asterisks*) development concerns the entire glomerulus. Due to the many pseudocysts, the glomerular tuft appears hypertrophied. **b** Enlarged view of a pseudocyst (*asterisk*), the floor of which is still made up of interdigitating foot processes (*arrows in the inset*). **c** Glomerular area with pseudocysts of different sizes (*asterisks*), the floor of which mostly shows foot process effacement (*arrow in the inset*). Note the varying density of pseudocyst content likely reflecting different albumin concentrations. The accumulation of intracellular vesicles (lysosomes) of varying density is also visible in injured podocytes (*arrowheads*). **d** Advanced stage of damage with many pseudocysts (*asterisks*) and many areas of bare GBM where podocytes were detached (*red dots*). At those sites, in addition to large pseudocysts (*asterisks*), secondary small pseudocysts (*enlarged in the inset*) have developed that regularly communicate with the large pseudocysts (not encountered in this section). Accumulations of intracellular vesicles in podocytes are also seen. **e** Tuft adhesion to Bowman's capsule. Podocytes with pseudocysts (*asterisks*) attach to the parietal epithelium (*P*) or parietal basement membrane (PBM; highlighted in *brown*). The integrity of the parietal epithelium is already lost; instead, fluid accumulation is seen (*star*). Outside the PBM loose connective tissue has settled. **F**: Advanced tuft adhesion to Bowman's

capsule accompanied with a break of the PBM and a displacement of the parietal epithelial cells (*P*) leading to an open connection between Bowman's and the interstital spaces (*curved arrows*). A peripheral capillary loop still covered by "effaced" podocyte portions (*arrow*) is attached to a group of (most likely) parietal cells (*star*); the mesangial stalk of this loop is deprived of podocytes (*arrowheads*). Other podocytes with pseudocysts (*asterisks*) adhere to the adhesion. *I*, interstitial cell; *PC*, peritubular capillary. Images of **a–d** were taken 4 days, images of **e** and **f** 8 days after PAN treatment. *Scale bars* = 10 μm (**a**), 5 μm (**d–f**), and 2 μm (**b**, **c**)

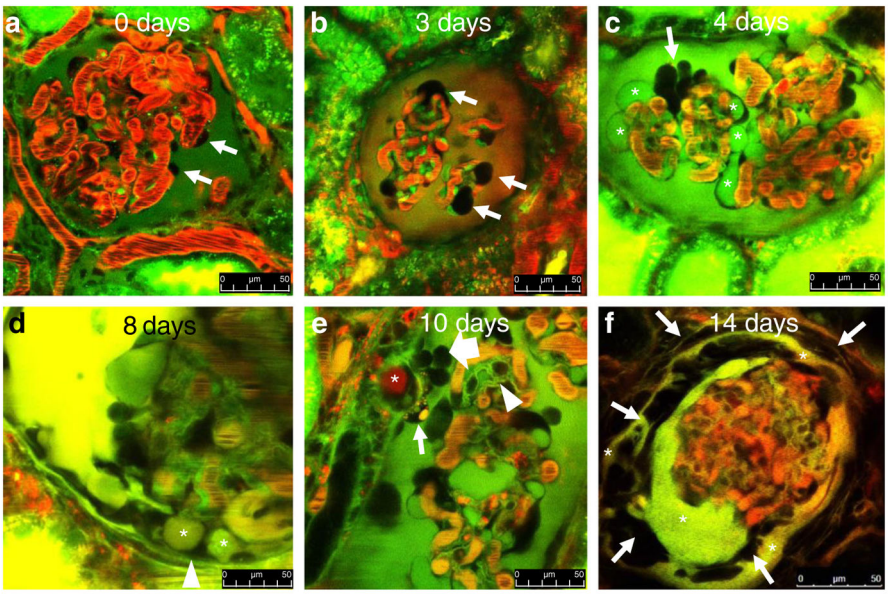

Fig. 2.

MPM imaging of the progression of glomerular pathology in vivo in a puromycin aminonucleoside (PAN)-induced model of FSGS in Munich-Wistar-Fromter rats. *Red*: intravascular space (plasma) marker Alexa 594-albumin given in iv bolus. Dark objects in red capillary plasma are red blood cells. *Green/yellow*: Lucifer yellow (LY) infused continuously into the carotid artery. In **b**, the nuclear stain Hoechst 33342 was also given iv to help the identification of various cells (*green*). The Bowman's space is labeled by the freely filtered LY identifying podocytes (*arrows*) and parietal cells (which do not take up the dye) based on negative labeling. **a** Normal glomerular morphology is visible at baseline. **b** Podocytes with enlarged, balled-up cell body (*arrows*) appear 2–3 days after PAN treatment. **c** In addition to enlarged podocytes (*arrow*), numerous large cysts are visible in dark, unlabeled podocytes (*asterisks*) 4 days after PAN treatment. **d** Podocyte pseudocysts *(asterisks*) are in contact with the parietal Bowman's capsule (*arrowhead*) at 8 days after PAN. **e** A fully formed adhesion (synechia) between the visceral and parietal Bowman's capsules appearing 10 days after PAN, formed by an albumin (*red*)-containing pseudocyst (*asterisk*) and surrounded by several tightly packed cells (*block arrow*) and a podocyte containing green/yellow/red-labeled vesicles (*arrow*). Glomerular basement membranes are also labeled green by LY (*arrowhead*). **f** Multilayered Bowman's capsule consisting of numerous cells (*arrows*) and LY-filled fluid spaces (*asterisks*) surrounds a barely perfused glomerulus (note the lack of red blood cells within glomerular capillaries) 14 days after PAN. *Scale bars* = 50 μm

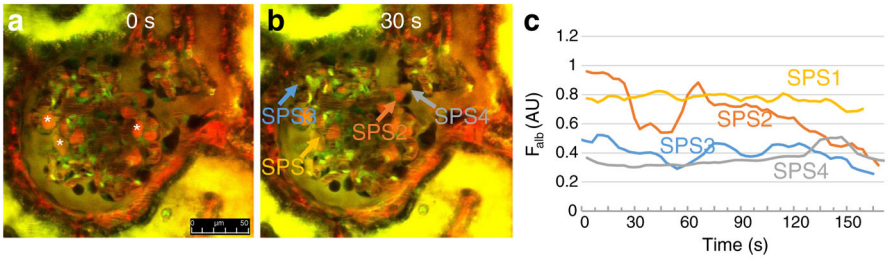

Fig. 3.

Time-lapse MPM imaging of the dynamics of podocyte pseudocyst volume changes in vivo in PAN-treated Munich-Wistar-Fromter rat kidneys. *Red*: Plasma marker Alexa 594-albumin. *Green*/*yellow*: Lucifer yellow (LY) infused continuously into the carotid artery to label the Bowman's space and to identify podocytes by negative labeling. Images taken 12 days after PAN treatment. Numerous albumin-containing (*red*) podocyte pseudocysts are visible in negatively labeled podocytes (*asterisks*). Compared to image taken at time zero (**a**), the volume of several pseudocysts increased or decreased within 30 s (**b**). **c** Time-dependent dynamic alterations in volume and albumin fluorescence intensity (F_{alb}) of four different podocyte pseudocysts as indicated by *color-matched arrows* in **b**. Also see Supplement movie 1 showing the same preparation. *Scale bar* = 50 μm

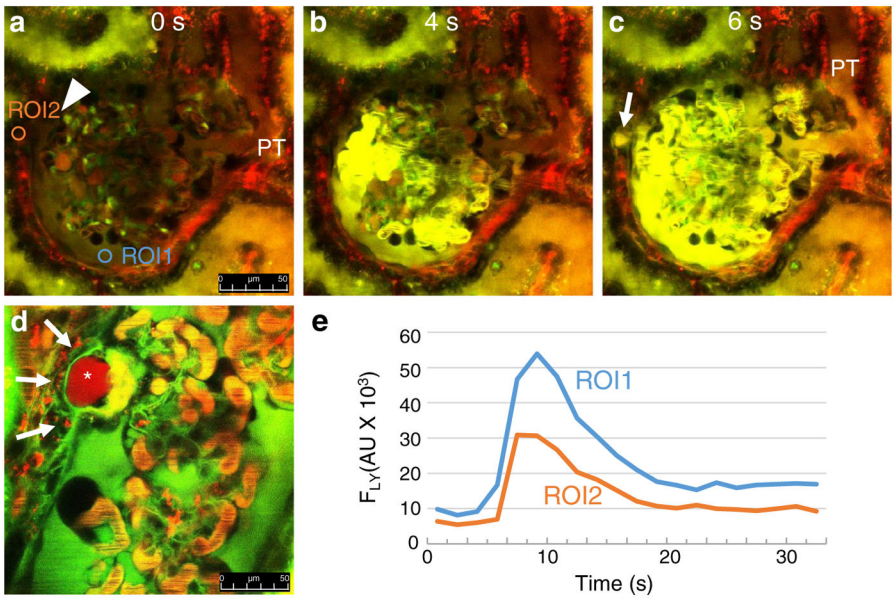

Fig. 4.

Time-lapse MPM imaging of misdirected filtration in vivo in PAN-treated Munich-Wistar-Fromter rat kidneys. *Red*: Plasma marker Alexa 594-albumin. *Green*/*yellow*: Freely filtered Lucifer yellow (LY) infused continuously into the carotid artery to label the primary filtrate. Images taken 12 days after PAN treatment. Glomerular leakage (*visible red* filtrate in Bowman's space marked by ROI2 in **a**) and proximal tubule (*PT*) uptake of albumin are visible after PAN treatment. An adhesion (synechia) appears between the visceral and parietal Bowman's capsule (*arrowhead*, **a**). Compared to the low background at time zero (**a**), bright LY fluorescence appears in glomerular capillaries and the Bowman's space within 4 s of initiating carotid infusion (**b**). **c** At 6 s, high LY fluorescence appears at a specific focal region outside the glomerulus adjacent to the synechia (*arrow*, *ROI1* in panel A), simultaneously with the initial filtration of LY into the Bowman's space and PT lumen. **d** High albumin (*red*)-containing pseudocyst (*asterisk*) in a synechia appears to filter albumin into the periglomerular interstitium, which is taken up by numerous cells surrounding this focal region (*arrows*). **e** Line plot of LY fluorescence intensity changes (F_{LY}) measured in two regions of interest (*ROI1* in the Bowman's space, and *ROI2* outside the glomerulus) as indicated in **a**. Also, see Supplement movies 2–3 showing the same preparations. *Scale bars* = 50 μm

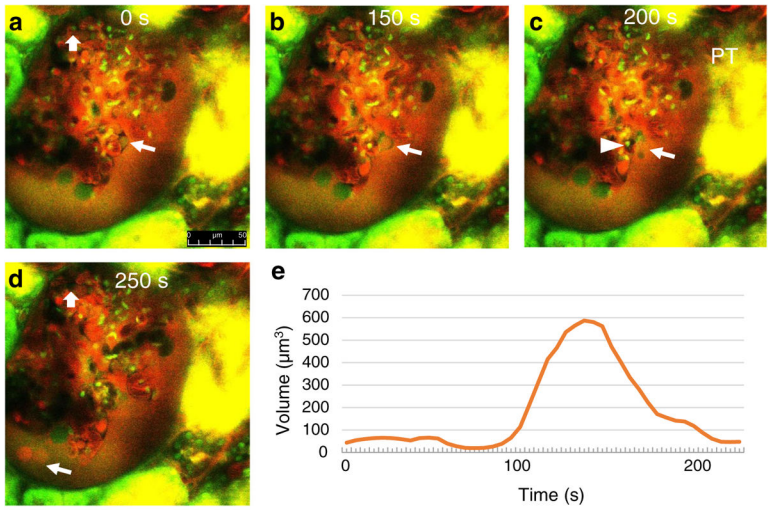

Fig. 5.

Time-lapse MPM imaging of podocyte shedding in vivo in PAN-treated Munich-Wistar-Fromter rat kidneys. *Red*: Plasma marker Alexa 594-albumin. *Green*/*yellow*: Lucifer yellow (LY) infused continuously into the carotid artery to label the primary filtrate. Hoechst 33342 identifies cell nuclei (*green*). Images taken 12 days after PAN treatment. Glomerular leakage of albumin is visible based on red filtrate in Bowman's space around glomerular capillaries. At time zero (**a**), a small pseudocyst is present in the labeled podocyte (*arrow*), and an intact endothelial cell is visible in a glomerular capillary (block arrow). **b** Within 150 s, the same pseudocyst is significantly enlarged. **c** At 200 s, the pseudocyst is ruptured and shedding of cell debris is visible (*arrow*). A microthrombus (dark capillary mass, no red plasma) developed in the glomerular capillary directly adjacent to the injured podocyte (*arrowhead*). **d** Albumin-containing (*red*) vesicles appear shedding into the filtrate at 250 s. Note the absence of the same endothelial cell labeled in **a**, replaced by a microthrombus (*block arrow*). **e** Dynamic changes in the volume of the podocyte pseudocyst labeled in **a–c**. Also, see Supplement movie 4 showing the same preparation. *Scale bar* = 50 µm